

Thermal Activated Reversible Phosphorescence Behavior of Solid Supramolecule Mediated by β -Cyclodextrin

Xiaolu Zhou, Xuan Zhao, Xue Bai, Qingwen Cheng, and Yu Liu*

A reversible solid thermally responsive deep-blue pure organic room temperature phosphorescent material is constructed by terephthalic acid (PPA), β -cyclodextrin (β -CD), and poly(vinylalcohol) (PVA). Attributed to the host-guest interaction of β -CD to isolate PPA chromophore and the rigid environment offered by hydrogen bonds to suppress the nonradiative decays, amorphous supramolecular assembly PPA-CD/PVA not only induces a deep-blue phosphorescence at 410 nm that differing from traditional PPA derivatives with green emission but also enhances the quantum yield up to 30.52%. Uncommonly, this film exhibits a unique reversible thermal stimulation response property with blue and cyan phosphorescence color transitions because heating can destroy the binding behavior between β -CD and PPA, resulting in redshift phosphorescence emission from PPA stacking. Additionally, with the incorporation of Rhodamine B (RhB) or Sulforhodamine 101 (SR101) into the supramolecular film, color-tunable phosphorescence from blue to white, yellow, and red relying on the thermal stimulation is realized through triplet-to-singlet Förster resonance energy transfer (TS-FRET) platform. These thermochromic phosphorescence materials are successfully applied in multilevel anticounterfeiting and information encryption, which provides a new simple approach for temperature-responsive TS-FRET multicolor luminescence supramolecular materials.

considerable attention for their wide application in the fields of biosensing,^[6] information encryption,^[7] anticounterfeiting^[8] and light emitting diode.^[9] Among them, the thermal driving mode has been a hot research topic owing to its superiority of low cost, simplicity, and in situ temperature modulation. Much effort has been devoted to developing thermochromic fluorescence materials, including dynamic fluorophore,^[10] supramolecular self-assembly systems,^[11] thermoresponsive polymers,^[12] composite matrix blends,^[13] molecular-engineering strategy,^[14] etc. Compared with fluorescence materials, pure organic room-temperature phosphorescence (RTP) materials possessing long lifetimes and large Stokes shifts provide the ability to differentiate luminescent components based on luminescence duration. Although many effective RTP systems have been explored, including heavy-atom effect,^[15] crystallization,^[16] self-assembly,^[17] polymerization,^[18] doping,^[19] and molecular aggregation,^[20] the majority of reported stimulus-response RTP materials currently are limited to triplet

exciton sensitivity to water and oxygen exhibiting the switch of the phosphorescence signal with a single phosphorescent emission color^[21] or utilizing molecular structure and special crystal morphology to achieve light/force-stimulus response.^[22] For instance, Li et al. reported a water-sensitive multicolored organic RTP polymeric system that enables visible and multiple anticounterfeiting.^[23] Zhao et al. developed and reported a series of ultraviolet irradiation-responsive dynamic ultralong organic phosphorescence systems applied in multilevel information encryption.^[24] Tian et al. reported a stimulation-response transformation of the organic one-component small molecule 1, 2-bis(4-alkoxybenzene) ethane-1, 2-dione between high-efficiency blue-yellow RTP by grinding or hot-annealing the crystals.^[25] However, thermally responsive phosphorescence materials, especially reversible multicolor thermochromic phosphorescent materials with high sensitivity to temperature have been rarely reported. Therefore, it is crucial to develop a new approach to fabricate an efficient, stable, and available thermally controllable phosphorescence system that responds to temperature stimuli.

Herein, we proposed a facile strategy for constructing deep blue efficient phosphorescence based on β -cyclodextrin (β -CD) confined chromophores taking terephthalic acid (PPA) as a

1. Introduction

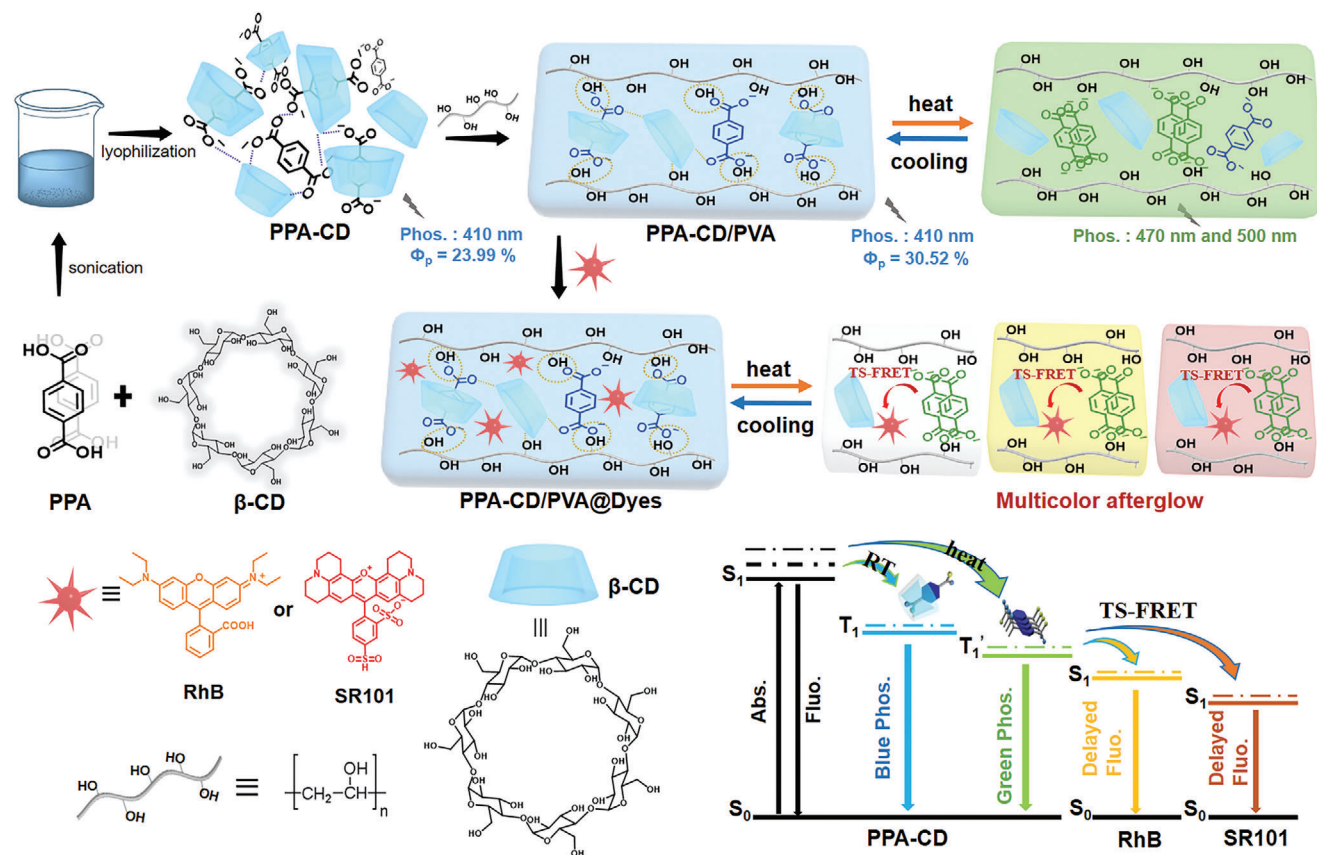
Stimulus-responsive color-tunable luminescent materials that quickly respond to external stimuli such as mechanical force,^[1] light,^[2] heat,^[3] pH,^[4] or solvent change^[5] have gained

X. Zhou, X. Zhao, X. Bai, Q. Cheng, Y. Liu
College of Chemistry
State Key Laboratory of Elemento Organic Chemistry
Nankai University
Tianjin 300071, P. R. China
E-mail: yuliu@nankai.edu.cn

Y. Liu
Collaborative Innovation Center of Chemical Science and Engineering
(Tianjin)
Nankai University
Tianjin 300071, P. R. China
Y. Liu
Haihe Laboratory of Sustainable Chemical Transformations
Tianjin 300071, P. R. China

 The ORCID identification number(s) for the author(s) of this article can be found under <https://doi.org/10.1002/adfm.202400898>

DOI: 10.1002/adfm.202400898



Scheme 1. Schematic illustration of PPA-CD, PPA-CD/PVA, and temperature stimulus response phosphorescence behavior and multicolor TS-FRET system.

model, which presents a thermally controlled reversible color-tunable phosphorescence behavior. The experimental results demonstrated that the encapsulation of β -CD and hydrogen bond interaction can effectively inhibit the nonradiative transition to improve the luminescence properties and avoid the redshifted emissions caused by molecular stacking of PPA. Accordingly, the assembly of PPA and β -CD (PPA-CD) displayed a deep-blue phosphorescence from isolated PPA chromophore with a high singlet state to triplet state conversion efficiency and a high quantum yield of 23.99%. The secondary assembly of PPA-CD and polyvinyl alcohol (PVA) provides a more rigid environment for the chromophore, further enhancing the phosphorescence property with a lifetime increase from 61.55 ms to 0.59 s and a quantum yield of up to 30.52%. Interestingly, the supramolecular film PPA-CD/PVA presented a unique reversible thermal stimulation response with blue and cyan phosphorescence color transitions, which was ascribed to the thermally controlled binding behavior of PPA and β -CD. Furthermore, by doping suitable fluorescent dyes (RhB, SR101) into supramolecular films, the thermal response afterglow color range was extended to white, yellow, and red regions through triplet-to-singlet Förster resonance energy transfer (TS-FRET) (Scheme 1). Finally, combined with the recognition and complexation of β -CD to PPA and its reversible thermal response properties, a series of information encryption and anticounterfeiting materials were developed. This finding not only opens up new research paths to construct amorphous

blue RTP materials but also provides a simple supramolecular platform to construct temperature-response multicolor afterglow RTP material.

2. Results and Discussion

Notoriously, β -CD, a macrocyclic host molecule with a long research history, not only can bind with some neutral molecules and anions to form a stable complex with stoichiometric ratios of 1:1 through hydrophobic interaction but also can induce or enhance the phosphorescence emission through macrocyclic confinement effect.^[26] In the present work, we demonstrated that based on the controllable β -CD confinement to isolate and restrict chromophores, the selective binding of β -CD and terephthalic acid could achieve an efficient blue phosphorescence with reversible color-tunable thermal stimulus-response character. A series of phthalic acid derivatives were chosen as the guest molecules and PPA as a model chromophore, which has a suitable molecule size that matches the cavity of β -CD providing prerequisites for host-guest complexation, and the carboxyl groups can hydrogen-bond with hydroxyl to form a rigid molecular network, ultimately suppressing molecular-vibration-induced non-radiative transition and facilitating the phosphorescence. The assembly of PPA-CD was obtained by sonicating and lyophilizing an aqueous mixture of PPA and β -CD (molar ratio = 1:1) with potassium carbonate-assisted dissolution (Figure 1a). The X-ray

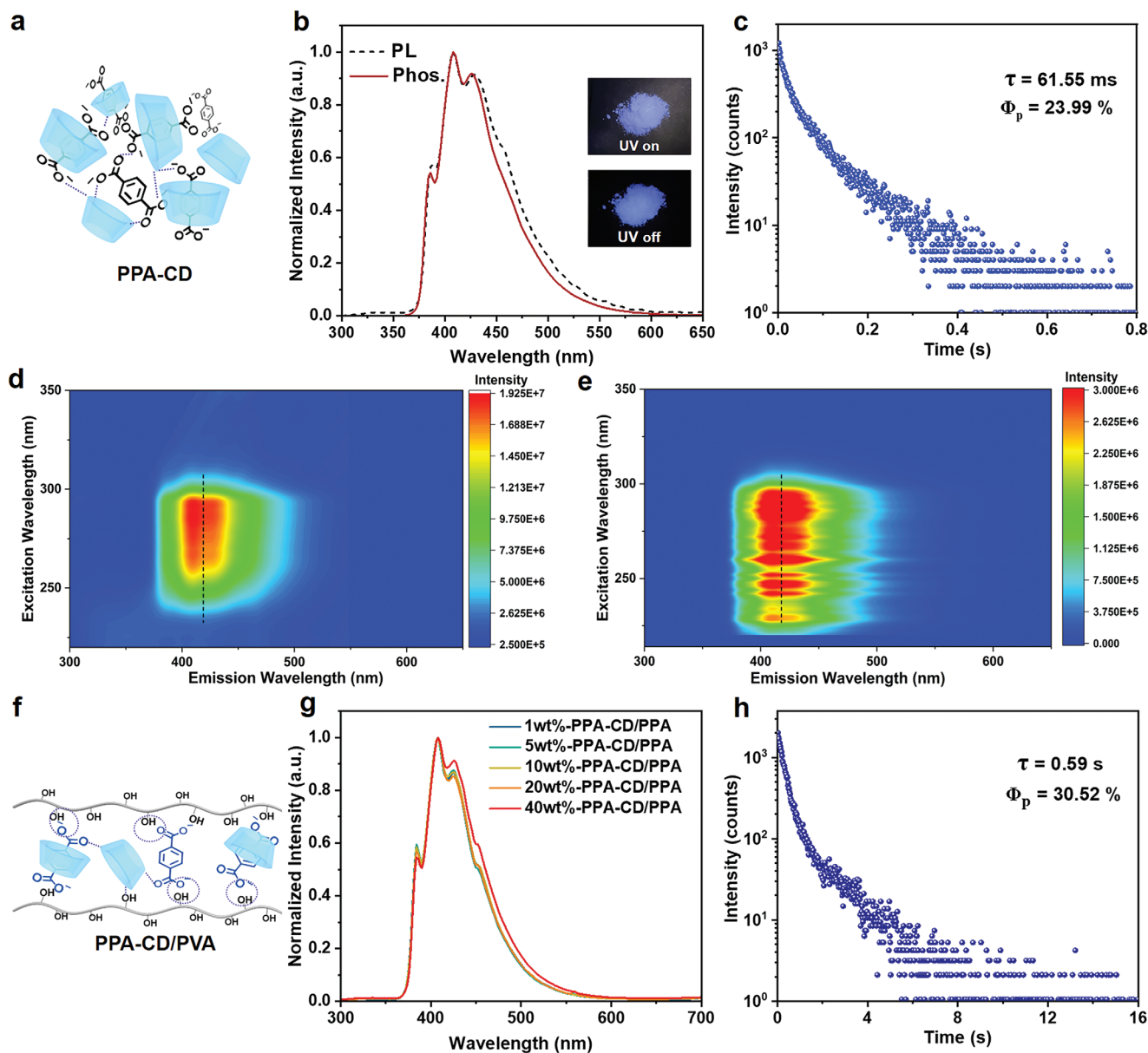


Figure 1. a) Chemical structure model of PPA-CD. b) Normalized steady-state PL (dashed black line) and phosphorescence (solid red line) spectra of PPA-CD powder ($\lambda_{\text{ex}} = 280$ nm). Inset: photographs of the PPA-CD under 300 nm UV irradiation (on/off). c) Time-resolved decay spectra were detected at 410 nm, and quantum yield for PPA-CD. d,e) Excitation-PL emission mapping d) and excitation-phosphorescence emission mapping e) of PPA-CD powder under ambient conditions. f) Schematic illustration of PPA-CD/PVA. g) Normalized steady-state PL spectra of the films of PPA-CD/PVA in different doping mass ratios ($\lambda_{\text{ex}} = 280$ nm). h) Time-resolved decay spectra and quantum yield of PPA-CD/PVA (The mass ratio of PPA and PVA is 1:20, the molar ratio of PPA and β -CD is 1:1) ($\lambda_{\text{ex}} = 280$ nm, recorded at 410 nm). (All phosphorescence spectra were recorded with a delay time of 1 ms.)

powder diffraction demonstrated that the freeze-dried PPA-CD powder was in an amorphous state (Figure S1, Supporting Information).

2.1. Photophysical Properties of PPA-CD and PPA-CD/PVA

As anticipated, PPA-CD exhibited a bright, deep-blue afterglow after cessation of 300 nm UV irradiation (Figure 1b inset). The steady-state PL and phosphorescence spectra of PPA-CD

showed almost identical emission peak curves presenting deep-blue emission at 410 nm (Figure 1b). The emission band in the PL spectrum at 317 nm was indicative of fluorescence with a lifetime recorded as 152.6 ps (Figure S2, Supporting Information), and the time-resolved PL spectrum monitored at 410 nm with a lifetime of 61.55 ms confirmed the phosphorescence nature of the blue afterglow (Figure 1c). The phosphorescence quantum efficiency of PPA-CD was acquired as 23.99% under ambient conditions, which surpassed most of the blue-RTP materials under ambient conditions. Both steady-state PL and phosphorescence

spectra showed the intense vibrational band at 410 nm excited from 220 to 350 nm (Figure 1d,e), excluding the red-shift emission caused by molecule coupling and indicating an effective singlet to triplet intersystem crossing (ISC).^[27] Additionally, a deep-blue peak at 420 nm was observed from the phosphorescence spectra of PPA in a dilute N, N-dimethylformamide at 80 K (Figure S3, Supporting Information), which were quite similar to that in PPA-CD at room temperature, indicating that the deep-blue phosphorescence emission of PPA-CD came from the luminescence of isolated PPA chromophore. Whereas the freeze-dried system PPA-K₂CO₃ exhibited a red-shifted phosphorescent emission at 500 nm (Figure S4, Supporting Information) caused by π - π stacking between neighboring chromophores,^[28] further confirming the phosphorescence effect of β -CD-confinement to isolate PPA chromophore. Subsequently, supramolecular assemblies containing different equivalent ratios between PPA and β -CD were synthesized and characterized to explore the effect of the host contents on the photoluminescence. As the equivalent ratio of PPA and CD is 1:0.5, the PL spectrum displayed a comparatively strong fluorescent peak at 317 nm, and when cyclodextrin was increased to one equivalent (Figure S5, Supporting Information), the efficient deep-blue phosphorescence can be achieved in a high conversion efficiency, preliminarily promulgating the formation process of β -CD-confined-isolated PPA chromophore.

Given the flexibility, machinability, and excellent film-forming ability of PVA, as well as the presence of abundant hydroxyl groups that can provide a rigid hydrogen bond network, this further limits the movement of the PPA-CD. We further co-assembled PPA-CD and PVA to construct a supramolecular polymer film (Figure 1f) and systematically investigated its photo-physical properties. Corresponding to the luminous property of PPA-CD in the solid packing state, the PL and phosphorescence spectra of PPA-CD/PVA films at different doping mass ratios of 1, 5, 10, 20, and 40 wt.% showed a uniform emission peak at 410 nm excited by 280 nm (Figure 1g; Figure S6, Supporting Information), indicating the stable existence of the assembly PPA-CD in PVA environment. Notably, the 5 wt.%-PPA-CD/PVA presented a higher phosphorescent quantum yield of 30.52% and a longer lifetime at 0.59 s than PPA-CD (Figure 1h), implying that the co-assembly of PPA-CD and PVA could significantly improve the phosphorescence properties. Additionally, the phosphorescence quantum yields of PPA-CD/polyacrylamide (PPA-CD/PAM), PPA-CD/sodium-polyacrylate (PPA-CD/PAS) and PPA-CD/polyethylene-glycol (PPA-CD/PEG) in a same molar ratio were determined to 26.22%, 10.03% and 4.26%, respectively, lower than that of PPA-CD/PVA (30.52%) (Figure S7, Supporting Information), indicating the importance of rigid hydrogen bond networks for improving the phosphorescence properties.^[29]

Due to the dynamic equilibrium assembly process between cyclodextrin and guests being susceptible to environmental temperature change, the thermal stimulation response property of PPA-CD/PVA was further explored. Surprisingly, PPA-CD/PVA film ($m_{\text{PPA}}:m_{\text{PVA}} = 1:5$) displayed a reversible thermally controlled phosphorescence behavior with afterglow color changing from blue to green under alternating heating and cooling stimuli (Figure 2a). As shown in Figure 2b, the normalized phosphorescence spectra of PPA-CD/PVA exhibited a unique emission peak of 410 nm at room temperature (25 °C) with no RTP emis-

sion in the long wavelength. However, as the heating temperature rose to 55 °C, the emission of 410 nm dropped sharply, accompanied by emerging emission bands of 470 and 500 nm. Accordingly, the afterglow photos of PPA-CD/PVA showed blue afterglow at room temperature and transformed to turquoise in a heating zone with good reciprocity (Figure 2d). The phosphorescence change curve of the heating and cooling process demonstrated that the phosphorescence spectrum of PPA-CD/PVA ($m_{\text{PPA}}:m_{\text{PVA}} = 1:5$) became stable after heating at 55 °C for ≈ 185 s, and could be restored after cooling for 140 s to 25 °C (Figure S8, Supporting Information). Even if the temperature dropped sharply, the film also could quickly return to a blue luminescence (Figure S9, Supporting Information). The heating-cooling cycle could be repeated many times (Figure 2c; Figure S10, Supporting Information), and the CIE coordinates of phosphorescence emission of PPA-CD/PVA at 25 and 55 °C were calculated as (0.17, 0.13) and (0.23, 0.31) respectively (Figure S11, Supporting Information).

2.2. Mechanism Analysis for the Blue RTP Emission and Thermal Stimulation Response

To explore the mechanism of the efficient blue RTP emission for PPA-CD/PVA, ¹H NMR spectra were first performed to analyze the host-guest binding behaviors between PPA and β -CD. In Figure S12 (Supporting Information), the proton on the phenyl groups experienced a shift toward low field upon gradual addition of β -CD, and the corresponding association constant (*K*s) of PPA-CD was obtained as 84.69 M⁻¹. In the control experiment, stachyose (ST) and maltohexaose (MY), which have wealthy hydroxyl groups without macrocyclic cavities, were chosen as the hosts to explore the effect of the hydrophobic cavity and compared with PPA-CD, the steady-state PL spectrum for the lyophilized powder of PPA/ST and PPA/MY displayed a low conversion efficiency in double emission consisting of a fluorescent peak at 317 nm and a phosphorescence peak at 410 nm (Figure 3a,b). Obvious poorer phosphorescence lifetime and quantum yield of PPA/ST ($\tau_p = 12.48$ ms, $\phi_p = 1.69\%$) and PPA/MY ($\tau_p = 33.42$ ms, $\phi_p = 2.18\%$) revealed the importance of the hydrophobic cavity's encapsulation that only hydrogen bonding interaction was insufficient to confine and isolate the PPA chromophore (Figure 3c,d). Moreover, although α -CD induced a better blue phosphorescence effect than ST and MY, it was still inferior to PPA-CD, exhibiting lower conversion efficiency and quantum yield at 3.97%, as well as a shorter phosphorescence lifetime of 51.00 ms, owing to a relatively weak corresponding association constant (*K*s = 18.62 M⁻¹) (Figure S13, Supporting Information). Besides the host-guest inclusion interaction, the hydrogen bonding interactions from the abundant hydroxyl group of β -CD also played a key role in developing this deep-blue phosphorescence. Methyl- β -cyclodextrin (PMe- β -CD) was chosen as the host to carry out the control experiment. As expected, the PPA/PMe- β -CD system displayed a weaker ISC process with double emission of fluorescence and phosphorescence compared with PPA-CD, the phosphorescence lifetime was recorded as 2.01 ms, and the quantum yield was obtained to be only 1.10% (Figure 3a-d). Thus, the synergistic effect of cavity encapsulation and hydrogen bonding interaction is the fundamental reason for realizing β -CD-confined deep blue RTP for

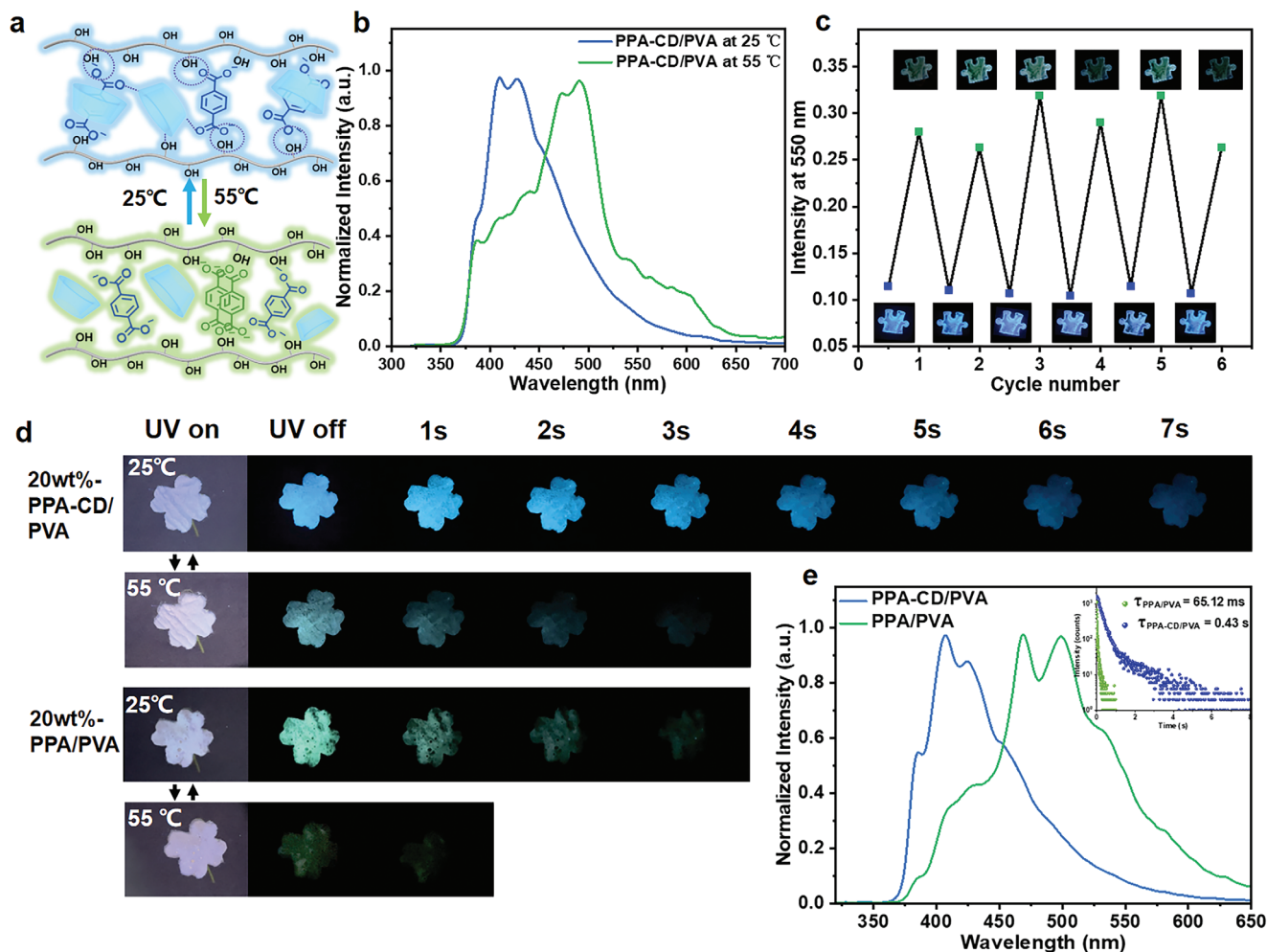


Figure 2. a) Schematic illustration of thermal response for PPA-CD/PVA. b) Normalized phosphorescence spectra of 20 wt.%-PPA-CD/PVA film ($\lambda_{\text{ex}} = 310$ nm, the mass ratio of PPA and PVA is 1:5, the molar ratio of PPA and β -CD is 1:1, Delay time = 5 ms). c) In repeated cycles, the emission intensity changes at 500 nm according to the normalized phosphorescence spectra of 20 wt.%-PPA-CD/PVA under 25 and 55 $^{\circ}\text{C}$, and the corresponding photographs of PPA-CD/PVA film after turning off the UV irradiation. d) The afterglow photographs of 20 wt.%-PPA-CD/PVA and 20 wt.%-PPA/PVA at 25 and 55 $^{\circ}\text{C}$, respectively. e) Normalized phosphorescence and time-resolved decay spectra of the films of 20 wt.%-PPA-CD/PVA and 20 wt.%-PPA/PVA. (Delay time = 5 ms).

isolated PPA moieties. Additionally, the Fourier transform infrared (FTIR) spectra of PPA/PVA exhibited a shorter wavelength at 3282 cm^{-1} than PPA-CD/PVA at 3301 cm^{-1} , which can be deduced that hydroxyl groups of β -CD strengthened the hydrogen bond association between the assembly and PVA resulting in a rigid network, thereby increasing RTP emissions (Figure S14, Supporting Information).

To explore the mechanism of the thermal-responsive RTP effect of PPA-CD/PVA film, PPA/PVA was prepared as a control. Under the same doping ratio ($m_{\text{PPA}}:m_{\text{PVA}} = 1:5$), the phosphorescence lifetime of PPA-CD/PVA was monitored as 0.43 s, which was longer than that of PPA/PVA ($\tau_{\text{p}} = 65.12$ ms), demonstrating the potential of β -CD assembly to inhibit nonradiative transition for enhancing phosphorescence properties for the guest molecule (Figure 2e). Notably, the thermochromic phosphorescence behavior did not occur in PPA/PVA ($m_{\text{PPA}}:m_{\text{PVA}} = 1:5$) film, where the phosphorescence spectrum after heating was almost identical to that at room temperature, only reflected in the change

of intensity (Figure S15, Supporting Information), due to the sensitivity of triplet excitons to temperature. In response, the afterglow color of PPA/PVA in a heating environment did not change and remained green (Figure 2d). Additionally, the PPA/PVA films under the low proportion of PPA doping ($m_{\text{PPA}}:m_{\text{PVA}} = 1:100, 1:20, 1:10$) also did not show a significant thermochromic behavior. (Figure S16, Supporting Information). It revealed the necessity for β -CD-confinement to achieve this reversible thermal stimulation response platform. The UV-vis absorption spectrum showed that the absorbance of PPA at room temperature presented a continuous increase trend with the addition of β -CD, indicating the complexation between β -CD and PPA (Figure S17a, Supporting Information). While the temperature rose to 55 $^{\circ}\text{C}$, the absorption peak of PPA-CD was significantly reduced, implying that the thermal environment weakened the host-guest interaction of PPA and β -CD (Figure S17b, Supporting Information). In addition, the Fourier transform infrared (FTIR) spectra were measured, in which PPA-CD exhibited a noticeable peak at

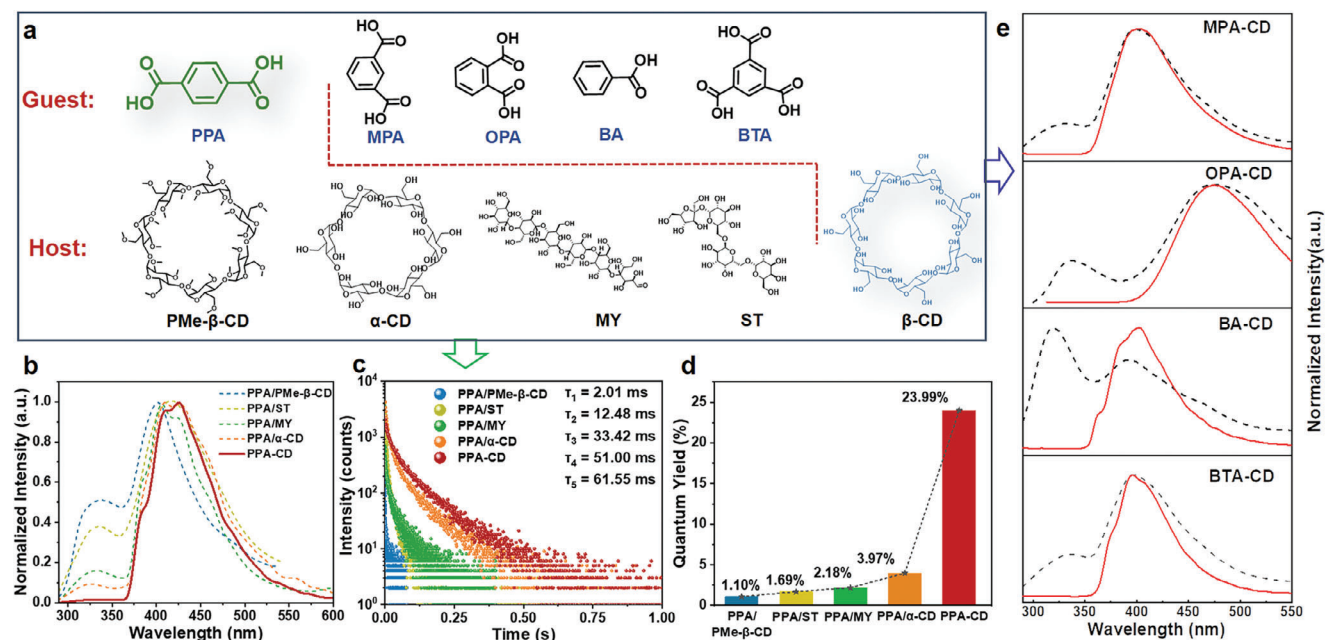


Figure 3. a) The chemical structures of phenyl-carboxylic acid derivatives as phosphorescent guests and macrocycles or oligosaccharides as hosts. b–d) Normalized steady-state PL spectra b), time-resolved decay spectra c), and quantum yield d) for the assembly of guest molecule PPA with different hosts. ($\lambda_{\text{ex}} = 280$ nm, recorded at 410 nm). e) Normalized steady-state PL (dashed black line) and phosphorescence (solid red line) spectra for the assembly of host molecule β -CD with different guests ($\lambda_{\text{ex}} = 280$ nm).

3250 cm^{-1} , and the peak intensity became notably weaker and narrower under heating conditions, proving that heat could reduce the degree of association of hydroxyl groups (Figure S18, Supporting Information). Moreover, the phosphorescence peaks of PPA-CD/PPA concentrated at 470 and 500 nm under thermal stimulation were consistent with the emission of the PPA/PPA film at room temperature, which should be attributed to the π - π stacking of PPA chromophores. Combined with the above experiment results, it was considered that the heating environment destroyed the confinement effect of β -CD through the destruction of host-guest interaction and hydrogen bond interaction, resulting in the accumulation of PPA molecules to produce redshifted RTP emission. On the contrary, host-guest complexation and hydrogen bonds were reconstructed after cooling the film, recovering the deep-blue RTP property. Therefore, the thermal sensitivity of PPA-CD/PPA film should be related to the destruction and reconstruction process of PPA-CD assembly.

Utterly, the universality of the β -CD-induced thermal stimulation response was investigated. The experimental results illustrated that the assembly of β -CD and other benzene carboxylic acid derivatives such as isophthalic acid (MPA), phthalic acid (OPA), benzoic acid (BA) and trimesic acid (BTA) also showed a blue RTP emission. As shown in Figure 3e, the PL and phosphorescence spectra showed emission peaks at 400, 470, 401, and 395 nm for MPA-CD, OPA-CD, BA-CD, and BTA-CD, respectively. The study of assembly for MPA with different host molecules showed a similar result to that of the PPA, in which MPA-CD has the highest optimal conversion efficiency and quantum yield relative to other macrocycles and oligosaccharides (Figure S19, Supporting Information), providing more convincing evidence for the cooperative effect of hydrophobic cavities and

hydrogen bonds in inducing blue phosphorescence. Moreover, the MPA-CD/PVA also showed excellent reversible thermal response performance. As shown in Figures S20 and S21 (Supporting Information), with temperature increasing from 25 to 75 $^{\circ}\text{C}$, the phosphorescent emission of MPA-CD/PVA gradually shifted from 410 to 500 nm, and the afterglow color gradually changed from blue to green, showing good repeatability in this thermal stimulus-response process.

2.3. Reversible PPA/Thermally Controlled TS-FRET System with Multicolor Afterglow

TS-FRET that transfers T_1 excitons of ultralong organic RTP emitters donor to S_1 excitons of fluorescent dyes has been proven to be an effective way to achieve tunable multicolor afterglow emission.^[30] To expand the thermal stimulation afterglow material, the TS-FRET system was constructed utilizing phosphors PPA-CD as energy donors and fluorescent dyes (RhB, SR101) as energy acceptors to regulate the afterglow color (Figure 4a). PPA-CD/PVA@RhB and PPA-CD/PVA@SR101 were prepared by doping rhodamine B and Sulforhodamine 101 into PPA-CD/PVA ($n_{\text{PPA}}: n_{\beta\text{-CD}} = 1:1.5$, $m_{\text{PPA}}:m_{\text{PVA}} = 1:5$). By adjusting the doping ratio of RhB and SR101, color-tunable emissions from blue to yellow were observed in PPA-CD/PVA@RhB and blue to red afterglow in PPA-CD/PVA@SR101. Correspondingly, the phosphorescence spectrum of PPA-CD/PVA@RhB showed two emission peaks at 410 and 575 nm, while the phosphorescence peaks of PPA-CD/PVA@SR101 mainly focused on 410 and 605 nm. Time-resolved emission-decay profiles revealed a distinct decrease in the PPA-CD lifetime upon increasing the

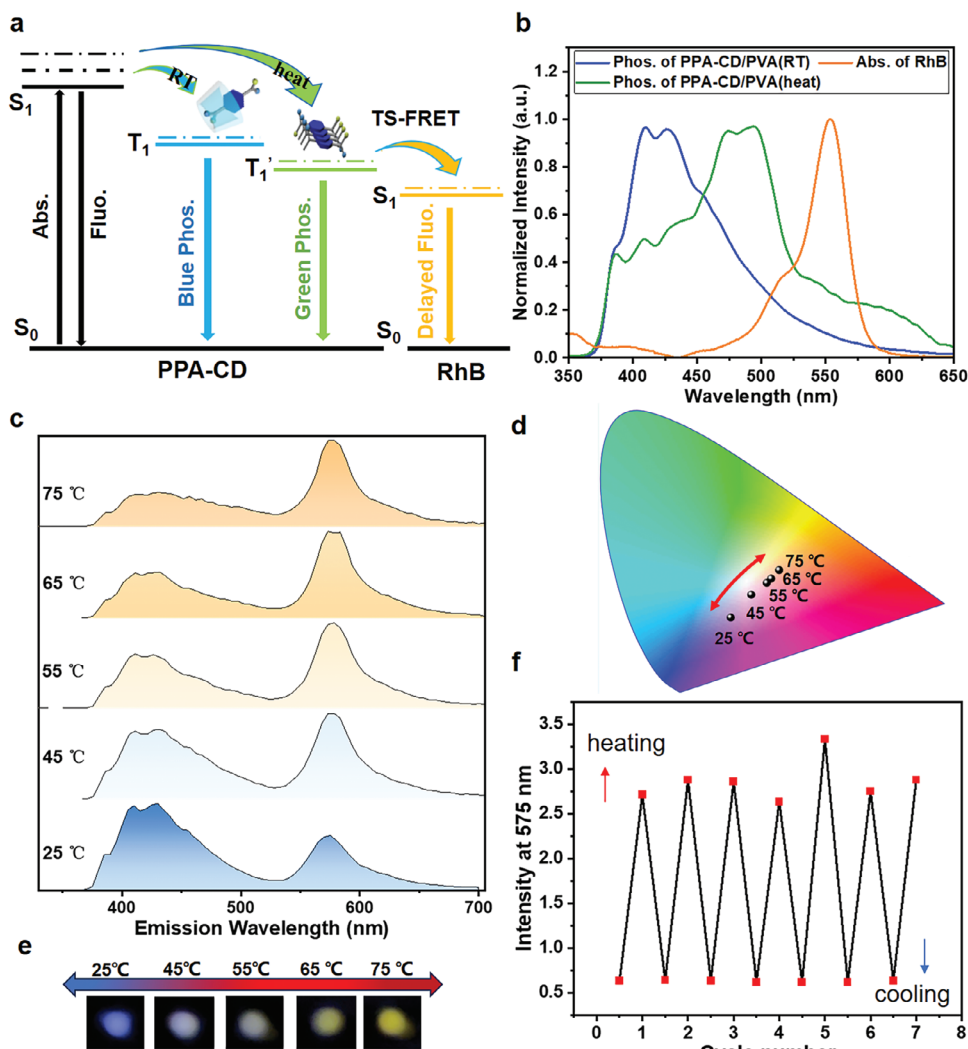


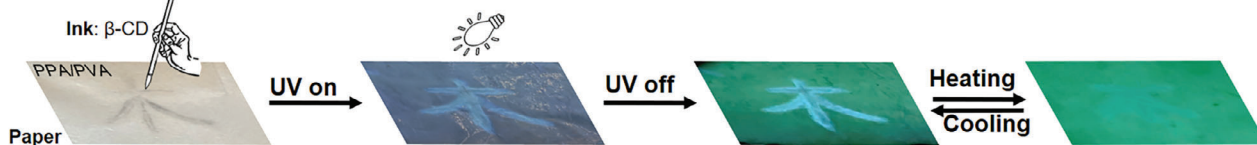
Figure 4. a) Simplified Jablonski diagram for temperature response multicolor TS-FRET system PPA-CD/PVA@RhB. b) Normalized phosphorescence spectrum ($\lambda_{\text{ex}} = 310$ nm, delayed time = 1 ms) of PPA-CD/PVA under room temperature (25 °C) and heat condition (55 °C) and normalized absorption spectra of the energy acceptors RhB in aqueous solution under ambient condition. c) Normalized phosphorescence spectra of PPA-CD/PVA@RhB ($\lambda_{\text{ex}} = 310$ nm, delayed time = 1 ms, $m_{\text{PPA}}:m_{\text{PVA}} = 1:5$, $n_{\text{PPA}}:n_{\beta\text{-CD}} = 1:1.5$, $n_{\text{PPA}}:n_{\text{RhB}} = 500:1$) under 25, 45, 55, 65, and 75 °C, respectively. d) CIE 1931 chromaticity diagram of afterglow color according to (c). e) Photographs of PPA-CD/PVA@RhB afterglow under 25, 45, 55, 65, and 75 °C. f) Emission intensity changes at 575 nm according to the normalized phosphorescence spectra (Figure S25b, Supporting Information) of PPA-CD/PVA@RhB under 25 and 75 °C.

doping ratio of fluorescent dyes, which provided further evidence for an effective TS-FRET (Figures S22 and S23, Supporting Information).

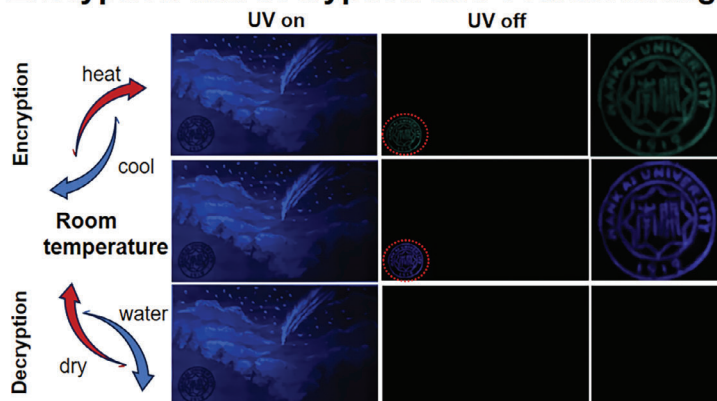
Considering that the phosphorescence spectrum of PPA-CD/PVA-55 °C film displayed a more significant overlap with the absorption spectra of RhB/SR101 than that of the PPA-CD/PVA-25 °C film, suggesting a more efficient energy transfer from triplet to singlet state (Figure 4b; Figure S24, Supporting Information). We took the doping film PPA-CD/PVA@RhB ($n_{\text{PPA-CD}}:n_{\text{RhB}} = 500:1$) as an example for thermal-responsive studies, and the corresponding emission color changes of the sample were monitored in situ. In the normalized phosphorescence spectrum of PPA-CD/PVA@RhB, as the temperature increased from 25 to 75 °C, the blue phosphorescence peak of 410 nm of PPA

monomer gradually decreased, and the peaks of 470 nm and 500 nm attributed to aggregated molecules appeared accompanied by an increased delayed fluorescence peak of RhB at 575 nm (Figure 4c). The calculated CIE coordinates showed a reversible transition from a blue to a yellow region (Figure 4d), and the heating-cooling response cycles can be repeated more than six times (Figure 4f; Figure S25, Supporting Information). The afterglow photo of PPA-CD/PVA@RhB presented blue at 25 °C, then changed to white at 45 °C and finally tuned to yellow at 65 °C, corresponding to the CIE coordinates (Figure 4e). Similarly, PPA-CD/PVA@SR101 ($n_{\text{PPA-CD}}:n_{\text{SR101}} = 200:1$) also exhibited multicolor luminescence in response to reversible thermal stimuli with afterglow color changing from blue to red as the temperature increased (Figure S26, Supporting Information). Therefore,

a Thermal stealth information material



b Encryption and decryption anti-counterfeiting



e Morse code with thermal controlled translation

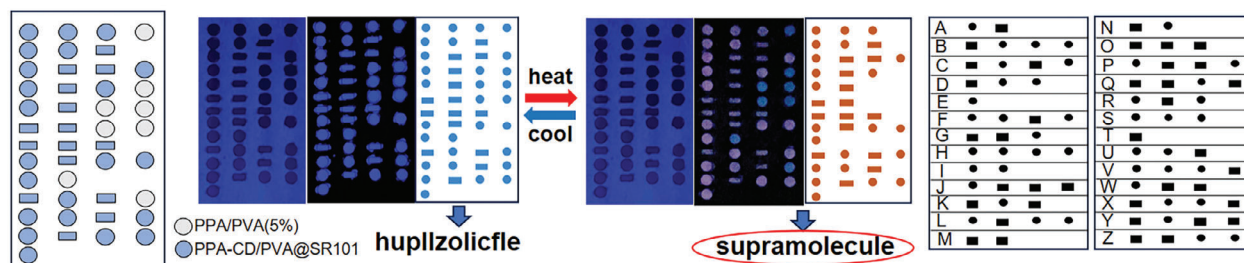


Figure 5. The schematic illustration of a) phosphorescence paper and ink for writable thermal stealth afterglow materials; b,c) Using seals to make anticounterfeiting marks and locally enlarged views of anticounterfeiting marks applied to thermal encryption and water decryption multiple anticounterfeiting; d) Cartoon anticounterfeiting signs in response to temperature stimuli; e) information encryption of Morse code with thermally controlled translation.

the TS-FRET platform can effectively amplify the thermal response property of PPA-CD/PVA to achieve a wide range of color adjustments, conductively expanding its practical application.

2.4. Application in Information Anticounterfeiting Material

Taking advantage of the excellent sensitivity to thermal response for PPA-CD/PVA and its processability, the application in temperature-oriented information storage and multi-level encryption were further studied. First, combined with the β -CD recognition and complexation to PPA, a thermal stealth information anticounterfeiting material was developed. As shown in **Figure 5a**, the paper was obtained by ordinary filter paper immersed in PPA/PVA solution, and the Chinese character “mu” (means tree) was written using β -CD as ink. After drying, the paper looked normal under visible light; however, after turning off the 300 nm ultraviolet excitation, the patterns of “mu” exhibited a blue afterglow while the background paper showed a green afterglow. In addition, the information of “mu” was hidden

in the green afterglow as heating and reappeared after cooling, mainly due to the co-assembly of β -CD and PPA isolated chromophores for blue phosphorescence and the thermal stimulation destroyed the binding behavior so that it could restore the aggregate green phosphorescence. Furthermore, PPA-CD/PVA can be used as a commercial anticounterfeiting ink for multiple anticounterfeiting encryptions of trademarks, calligraphy, and painting. As shown in **Figure 5b–d**, after stopping the ultraviolet excitation, a blue logo of “Nankai University” appeared and turned green when heated, and then resumed after cooling, which realized the encryption process. After fumigation with water, the logo’s afterglow disappeared, and the blue afterglow can be restored after drying to realize the decryption process. Last, under the thermal response multicolor afterglow characteristic of the PPA-CD/PVA@Dye system, a fast thermally controlled translation information encryption was developed, taking Morse code as an example (**Figure 5e**). According to the Morse code meter, after turning off the ultraviolet lamp of 300 nm, the error message “hupllzolicfle” was observed at room temperature, and when the temperature was increased to 65 °C, the correct hidden information

“supramolecule” was obtained. That was because PPA/PVA at a low PPA doping concentration has a blue phosphorescence emission without temperature-dependent luminous color change, whereas PPA-CD/PVA@SR101 has thermochromic phosphorescence and the afterglow color could change from blue to red as the temperature increases. This thermally translated Moss cipher has broad application potential as an international unified cipher.

3. Conclusion

In summary, we have successfully constructed a supramolecular thermally controlled blue RTP material based on β -CD. Benefiting from the hydrophobic cavities and abundant hydrogen bonds, β -CD can effectively isolate and restrict PPA chromophore, thus inhibiting its nonradiative transitions for efficient deep-blue phosphorescence. The co-assembly with PVA to obtain flexible processable supramolecular assembled films enhances the phosphorescent properties relying on hydrogen bond networks. In particular, the macrocyclic confined single molecule effects can regulate the luminescence behavior through temperature response. Moreover, by doping suitable fluorescent dyes in supramolecular systems to construct the TS-FRET platform, multicolor-tunable phosphorescence behavior can be achieved in these films by varying the acceptor doping ratio or temperature. The thermally controlled binding mode of PPA and β -CD is responsible for the luminescent thermochromism and temperature-modulated TS-FRET. This work provides an attractive alternative for constructing efficient blue phosphorescence and achieving multicolor thermal-stimulus phosphorescence behavior, which is potentially applied in temperature-oriented information storage, multicolor display, and multilevel encryption.

4. Experimental Section

Materials: All reagents and solvents were available from commercial sources and used directly without any purification. The PVA was purchased from Macklin ($M_w \approx 200\,000$).

Preparation of Supramolecular Assembly PPA-CD: PPA (13.28 mg, 0.08 mmol), β -CD (90.80 mg, 0.08 mmol), and K_2CO_3 (26.56 mg) were added to water (4 mL) and sonicated for 2 h. The aqueous solution was then lyophilized, and the white powder was obtained by further vacuum drying. Similar to the above preparation method, PPA/PMe- β -CD, PPA/ α -CD, PPA/ST, PPA/MY, MPA-CD, OPA-CD, BA-CD, BTA-CD were prepared with a stoichiometric ratio of host and guest at 1:1.

Preparation of Supramolecular Films 20 wt.-%-PPA-CD/PVA: A stirred solution of PPA (4 mg, 0.024 mmol), β -CD (27.35 mg, 0.024 mmol), and K_2CO_3 (8 mg) in water (1.6 mL), and 10% PVA water solution (200 μ L) was added. The mixture was stirred for 2 h. Then take 0.5 mL of the resulting mixed solution and drop it on the tinfoil with a syringe. Heat the tinfoil until the water evaporates.

Preparation of PPA-CD/PVA@RhB and PPA-CD/PVA@SR101 Films: The donor liquid PPA-CD/PVA ($n_{PPA} : n_{\beta-CD} = 1:1.5$, $m_{PPA} : m_{PVA} = 1:5$) was prepared by PPA (40 mg, 0.24 mmol), β -CD (410 mg, 0.36 mmol), K_2CO_3 (80 mg), water (16 mL) and 10% PVA water solution (2 mL). Take the donor solution of 0.3 mL and add dye molecules (RhB or SR101) according to different molar ratios. Then, the mixture was ultrasound for 2 h. Finally, drop 0.3 mL of the resulting mixed solution on the tinfoil with a syringe. Heat the tinfoil until the water evaporates.

Characterization: UV-vis absorption was kept details on Shimadzu UV-3600 spectrophotometer with a PTC-348WI temperature controller at 298 K. Photoluminescence (PL) spectrum and time-correlated decay profiles were documented on Edinburgh Instruments FS5 (Livingstone, UK).

The luminescent photos were taken by iPhone 13 under the irradiation of a UV lamp at room temperature. The powder X-ray diffraction patterns were obtained on Rigaku SmartLab. Fourier transform infrared (FTIR) spectra were determined by Thermofisher Scientific Nicolet iS5.

Supporting Information

Supporting Information is available from the Wiley Online Library or from the author.

Acknowledgements

The authors thank the National Nature Science Foundation of China (NNSFC, Grant Nos. 22131008), China Fundamental Research Funds for the Central Universities, and the Haihe Laboratory of Sustainable Chemical Transformations for financial support.

Conflict of Interest

The authors declare no conflict of interest.

Data Availability Statement

The data that support the findings of this study are available from the corresponding author upon reasonable request.

Keywords

pure organic room temperature phosphorescence, supramolecular assembly, thermal stimulation response, triplet-to-singlet Förster resonance energy transfer, β -cyclodextrin

Received: January 16, 2024

Revised: February 29, 2024

Published online:

- [1] a) F. Yang, T. Geng, H. Shen, Y. Kou, G. Xiao, B. Zou, Y. Chen, *Angew. Chem., Int. Ed.* **2023**, *62*, e202308662; b) Y. Sagara, T. Kato, *Nat. Chem.* **2009**, *1*, 605.
- [2] a) M.-M. Russew, S. Hecht, *Adv. Mater.* **2010**, *22*, 3348; b) H.-Q. Zheng, Y. Yang, Z. Wang, D. Yang, G. Qian, Y. Cui, *Adv. Mater.* **2023**, *35*, 2300177.
- [3] a) X. Bi, Y. Shi, T. Peng, S. Yue, F. Wang, L. Zheng, Q.-E. Cao, *Adv. Funct. Mater.* **2021**, *31*, 2101312; b) J. Troyano, O. Castillo, J. I. Martínez, V. Fernández-Moreira, Y. Ballesteros, D. MasPOCH, F. Zamora, S. Delgado, *Adv. Funct. Mater.* **2018**, *28*, 1704040.
- [4] a) S. Chen, Y. Hong, Y. Liu, J. Liu, C. W. T. Leung, M. Li, R. T. K. Kwok, E. Zhao, J. W. Y. Lam, Y. Yu, B. Z. Tang, *J. Am. Chem. Soc.* **2013**, *135*, 4926; b) Y. Bao, H. De Keersmaecker, S. Corneillie, F. Yu, H. Mizuno, G. Zhang, J. Hofkens, B. Mendrek, A. Kowalczyk, M. Smet, *Chem. Mater.* **2015**, *27*, 3450.
- [5] a) C. Wang, Q. Qiao, W. Chi, J. Chen, W. Liu, D. Tan, S. McKechnie, D. Lyu, X.-F. Jiang, W. Zhou, N. Xu, Q. Zhang, Z. Xu, X. Liu, *Angew. Chem., Int. Ed.* **2020**, *59*, 10160; b) R. Hu, E. Lager, A. Aguilar-Aguilar, J. Liu, J. W. Y. Lam, H. H. Y. Sung, I. D. Williams, Y. Zhong, K. S. Wong, E. Peña-Cabrera, B. Z. Tang, *J. Phys. Chem. C* **2009**, *113*, 15845.
- [6] N. Jiang, J. Fan, F. Xu, X. Peng, H. Mu, J. Wang, X. Xiong, *Angew. Chem., Int. Ed.* **2015**, *54*, 2510.

- [7] J. Wang, M. Zhang, S. Han, L. Zhu, X. Jia, *J. Phys. Chem. C* **2022**, *10*, 15565.
- [8] Z. Li, G. Wang, Y. Ye, B. Li, H. Li, B. Chen, *Angew. Chem., Int. Ed.* **2019**, *58*, 18025.
- [9] J. Zhang, Q. Zou, H. Tian, *Adv. Mater.* **2013**, *25*, 378.
- [10] a) D. Hu, W. Xu, G. Wang, K. Liu, Z. Wang, Q. Shi, S. Lin, Z. Liu, Y. Fang, *Adv. Funct. Mater.* **2022**, *32*, 2207895; b) F. D. Stefani, C. Kohl, Y. S. Avlasevich, N. Horn, A. K. Vogt, K. Müllen, M. Kreiter, *Chem. Mater.* **2006**, *18*, 6115.
- [11] D. Yan, J. Lu, J. Ma, M. Wei, D. G. Evans, X. Duan, *Angew. Chem., Int. Ed.* **2011**, *50*, 720.
- [12] a) Z. Qiu, E. K. K. Chu, M. Jiang, C. Gui, N. Xie, W. Qin, P. Alam, R. T. K. Kwok, J. W. Y. Lam, B. Z. Tang, *Macromolecules* **2017**, *50*, 7620; b) A. Seeboth, D. Löttsch, R. Ruhmann, O. Muehling, *Chem. Rev.* **2014**, *114*, 3037.
- [13] a) W. H. Yao, R. C. Lan, K. X. Li, L. Y. Zhang, *ACS Appl. Mater. Interfaces* **2021**, *13*, 1424; b) J. Du, L. Sheng, Q. Chen, Y. Xu, W. Li, X. Wang, M. Li, S. X.-A. Zhang, *Mater. Horiz.* **2019**, *6*, 1654.
- [14] K. Zhang, X. Zhou, S. Li, L. Zhao, W. Hu, A. Cai, Y. Zeng, Q. Wang, M. Wu, G. Li, J. Liu, H. Ji, Y. Qin, L. Wu, *Adv. Mater.* **2023**, *35*, 2305472.
- [15] a) H. Shi, L. Song, H. Ma, C. Sun, K. Huang, A. Lv, W. Ye, H. Wang, S. Cai, W. Yao, Y. Zhang, R. Zheng, Z. An, W. Huang, *J. Phys. Chem. Lett.* **2019**, *10*, 595. b) J. Wang, X. Gu, H. Ma, Q. Peng, X. Huang, X. Zheng, S. H. P. Sung, G. Shan, J. W. Y. Lam, Z. Shuai, B. Z. Tang, *Nat. Commun.* **2018**, *9*, 2963.
- [16] a) Y. Gong, G. Chen, Q. Peng, W. Z. Yuan, Y. Xie, S. Li, Y. Zhang, B. Z. Tang, *Adv. Mater.* **2015**, *27*, 6195; b) J. Yang, X. Zhen, B. Wang, X. Gao, Z. Ren, J. Wang, Y. Xie, J. Li, Q. Peng, K. Pu, Z. Li, *Nat. Commun.* **2018**, *9*, 840.
- [17] a) X. Yu, W. Liang, Q. Huang, W. Wu, J. J. Chruma, C. Yang, *Chem. Commun.* **2019**, *55*, 3156; b) X.-K. Ma, X. Zhou, J. Wu, F.-F. Shen, Y. Liu, *Adv. Sci.* **2022**, *9*, 2201182.
- [18] L. Gu, H. Wu, H. Ma, W. Ye, W. Jia, H. Wang, H. Chen, N. Zhang, D. Wang, C. Qian, Z. An, W. Huang, Y. Zhao, *Nat. Commun.* **2020**, *11*, 944.
- [19] a) D. Lee, O. Bolton, B. C. Kim, J. H. Youk, S. Takayama, J. Kim, *J. Am. Chem. Soc.* **2013**, *135*, 6325; b) W. Qiao, M. Yao, J. Xu, H. Peng, J. Xia, X. Xie, Z. a. Li, *Angew. Chem., Int. Ed.* **2023**, *62*, e202315911.
- [20] S. Cai, H. Shi, J. Li, L. Gu, Y. Ni, Z. Cheng, S. Wang, W.-w. Xiong, L. Li, Z. An, W. Huang, *Adv. Mater.* **2017**, *29*, 1701244.
- [21] a) F. Peng, Y. Chen, H. Liu, P. Chen, F. Peng, H. Qi, *Adv. Mater.* **2023**, *35*, 20234032; b) W.-T. Fan, Y. Chen, J. Niu, T. Su, J.-J. Li, Y. Liu, *Adv. Photonics Res.* **2021**, *2*, 2000080; c) Z. Q. Cheng, X. Wang, J. C. Zhao, S. Wang, X. F. Wu, H. Tong, L. X. Wang, *Macromolecules* **2023**, *56*, 2972.
- [22] a) J. Ren, Y. Wang, Y. Tian, Z. Liu, X. Xiao, J. Yang, M. Fang, Z. Li, *Angew. Chem., Int. Ed.* **2021**, *60*, 12335; b) Y. Wang, J. Yang, M. Fang, Y. Gong, J. Ren, L. Tu, B. Z. Tang, Z. Li, *Adv. Funct. Mater.* **2021**, *31*, 2101719; c) S. Xiong, Y. Xiong, D. Wang, Y. Pan, K. Chen, Z. Zhao, D. Wang, B. Z. Tang, *Adv. Mater.* **2023**, *35*, 20231874.
- [23] D. Li, Y. Yang, J. Yang, M. Fang, B. Z. Tang, Z. Li, *Nat. Commun.* **2022**, *13*, 347.
- [24] Y. F. Zhang, L. Gao, X. Zheng, Z. H. Wang, C. L. Yang, H. L. Tang, L. J. Qu, Y. B. Li, Y. L. Zhao, *Nat. Commun.* **2021**, *12*, 2297.
- [25] J. Song, L. Ma, S. Sun, H. Tian, X. Ma, *Angew. Chem., Int. Ed.* **2022**, *61*, e202206157.
- [26] a) D. Li, Z. Liu, M. Fang, J. Yang, B. Z. Tang, Z. Li, *ACS Nano* **2023**, *17*, 12895; b) D. Li, F. Lu, J. Wang, W. Hu, X.-M. Cao, X. Ma, H. Tian, *J. Am. Chem. Soc.* **2018**, *140*, 1916.
- [27] S. Xu, W. Wang, H. Li, J. Zhang, R. Chen, S. Wang, C. Zheng, G. Xing, C. Song, W. Huang, *Nat. Commun.* **2020**, *11*, 4802.
- [28] a) Y. Gong, L. Zhao, Q. Peng, D. Fan, W. Z. Yuan, Y. Zhang, B. Z. Tang, *Chem. Sci.* **2015**, *6*, 4438; b) X. Yang, D. Yan, *Adv. Opt. Mater.* **2016**, *4*, 897.
- [29] Y. Zhang, Y. Su, H. Wu, Z. Wang, C. Wang, Y. Zheng, X. Zheng, L. Gao, Q. Zhou, Y. Yang, X. Chen, C. Yang, Y. Zhao, *J. Am. Chem. Soc.* **2021**, *143*, 13675.
- [30] a) A. Kirch, M. Gmelch, S. Reineke, *J. Phys. Chem. Lett.* **2019**, *10*, 310; b) S. Kuila, S. J. George, *Angew. Chem., Int. Ed.* **2020**, *59*, 9393.